



## A three-dimensional analytic model for the scattering of a spherical bush

Robert E. Dickinson,<sup>1</sup> Liming Zhou,<sup>1</sup> Yuhong Tian,<sup>2,3</sup> Qing Liu,<sup>1</sup> Thomas Lavergne,<sup>4</sup> Bernard Pinty,<sup>4</sup> Crystal B. Schaaf,<sup>5</sup> and Yuri Knyazikhin<sup>5</sup>

Received 2 November 2007; revised 18 July 2008; accepted 28 July 2008; published 25 October 2008.

[1] Advanced climate models require a more realistic description of canopy radiation with reasonable computational efficiency. This paper develops the mathematics of scattering from a spherical object conceptualized to be a spherical bush to provide a building block that helps to address this need of climate models. It is composed of a homogeneous distribution of individual smaller objects that scatter isotropically. In the limit of small optical depth, incident radiation will scatter isotropically as the sum of that scattered by all the individual scatterers, but at large optical depth the radiation leaving the spherical bush in a given direction is reduced by mutual shadowing of the smaller objects. In the single scattering limit, the scattering phase function and so the albedo are obtained by simple but accurate analytic expressions derived from analytic integration and numerical evaluation. Except in the limit of thin canopies, the scattering and hence albedos are qualitatively and quantitatively different than those derived from 1-D modeling.

**Citation:** Dickinson, R. E., L. Zhou, Y. Tian, Q. Liu, T. Lavergne, B. Pinty, C. B. Schaaf, and Y. Knyazikhin (2008), A three-dimensional analytic model for the scattering of a spherical bush, *J. Geophys. Res.*, *113*, D20113, doi:10.1029/2007JD009564.

### 1. Introduction: The Importance of Addressing Three-Dimensional Radiation in Climate Models

[2] The surface energy, water and carbon balances at the terrestrial surface are controlled by absorption of incident solar radiation. Climate models currently describe this absorption in terms of a canopy architecture that can be highly unrealistic and inaccurate. If they constrain their absorption of radiative energy by accurate satellite observations of albedo [e.g., *Lucht et al.*, 2000; *Schaaf et al.*, 2002; *Wang et al.*, 2004; *Tian et al.*, 2004; *Liang et al.*, 2005; *Lawrence and Chase*, 2007], their solar forcing over the land surface should be of comparable accuracy. However, details as to how this absorbed radiation is partitioned between various components of the terrestrial system may still be determined very inaccurately, possibly resulting in deficiencies of the climate simulation.

[3] For example, forests overlying snow have been assumed through their contribution to absorption to increase surface temperatures from that of a forest free surface [e.g., *Bonan et al.*, 1992; *Betts et al.*, 2007] and so contribute to the melting of the snow. However, such a forest is also

directly removing incident solar energy from the snow and so, without some further energy exchange mechanism such as downward sensible and long-wave fluxes, would be shadowing and cooling the snow, not melting it. Semiarid or other sparsely vegetated systems have bushes that shade a much larger area than that of their vertical projection, an effect that can only be accounted for in a three-dimensional (3-D) geometry. Widely spaced individual bushes have no radiative effect on each other and can be treated in isolation, the topic of this paper.

[4] Detailed numerical treatments of the canopy radiation in complex 3-D geometries have been developed by various authors, mostly for application to remote sensing [e.g., *Myneni et al.*, 1995; *Knyazikhin et al.*, 1998; *Lewis*, 1999; *Qin and Gerstl*, 2000; *Kimes et al.*, 2002; *Li et al.*, 1995], but these treatments have not been translated into simple rules suitable for climate models. Rather, 1-D treatments [e.g., *Dickinson*, 1983; *Sellers*, 1985] have been popular because they are simple enough to require the evaluation of at most a few exponentials. An overall objective of our research is to establish how much of canopy radiation in 3-D can be described with comparable simplicity. Radiation within a canopy is, in principle, complicated by the multiple reflections between canopy elements and with the underlying surface. However, over the visible part of the solar spectrum, the contributions from multiple scattering are small. They can be taken as a separate component to be added to the single scattering of a canopy [e.g., *Pinty et al.*, 2006; *Knyazikhin et al.*, 2005]. Radiation leaving a canopy is completely characterized by its scattering phase function  $\Psi$ , i.e., given by the product of the phase function provided by individual leaves [cf. *Pinty et al.*, 2006] and the contribution from the shading by the distribution of leaves.

<sup>1</sup>School of Earth and Atmospheric Sciences, Georgia Institute of Technology, Atlanta, Georgia, USA.

<sup>2</sup>I.M. Systems Group, Inc., Rockville, Maryland, USA.

<sup>3</sup>Center for Satellite Applications and Research, NESDIS, NOAA, Camp Springs, Maryland, USA.

<sup>4</sup>Global Environmental Monitoring Unit, Institute for Environment and Sustainability, European Commission Joint Research Centre, Ispra, Italy.

<sup>5</sup>Department of Geography, Boston University, Boston, Massachusetts, USA.

[5] This paper addresses the latter issue. Thus, it furthers the approach of constructing scattered canopy radiation from individual geometric objects as pioneered by *Li et al.* [1995] with the intent of making it useful in climate models. Some more recent studies have shown how to mimic the effects of canopy heterogeneity on albedo in a horizontally layered framework. *Pinty et al.* [2006], use effective leaf optical properties and leaf area (LAI) as fitting parameters to match albedos from simulations with the Monte Carlo code of *Govaerts and Verstraete* [1998], *Shabanov et al.* [2000] and *Huang et al.* [2007a, 2007b] prescribe statistical distributions of path lengths through the canopy.

[6] This paper describes elementary analytic solutions for transmission and single scattering from a unit sphere comprised of individual scattering elements. These solutions are constructed in the absence of any other surface, i.e., they give the radiation scattered directionally by a sphere underlain by a black surface, an important building block for the construction of the domain averaged fluxes of radiative energy reflected from a heterogeneously vegetated surface. Modifications for leaf orientation effects, the multiply scattered component, the exchanges with an underlying flat surface such as soil or snow, and the effects of mutual shading (i.e., overlapping shadows) by a distribution of such spheres are also needed but their details are not given here; for similar issues in the context of clouds, see *Petty* [2002].

## 2. Formulation of Optical Paths and Scattering for a 3-D Canopy

[7] A detailed description of a bush would include its spatial dimensions and spatial distribution of leaf densities. However, such information is not commonly available even for a single location and cannot be expected to be provided to a climate model. Rather, the bush is characterized by an integral property, its leaf area index, i.e., the average leaf flat surface per unit ground area, where the latter can be either that under the bush or total area. This information is combined with information about the projection of the leaf surfaces in the direction of the radiation to construct optical depths.

[8] Radiation of unit intensity is assumed to be incident on a sphere of unit radius whose axis is taken to lie in the direction of this radiation (Figure 1). This geometry provides a variety of individual optical depths that are summarized in terms of a volume average optical depth  $\tau_v$ . Rather than directly use this parameter, it is more convenient to use the radial optical depth  $\tau = 0.75 \tau_v$  as is commonly done in treating radiation in spherical geometries. The underlying surface is assumed to be black and can have any orientation relative to the direction of incident light. The scattering properties for the so constructed object will allow later addition of the contribution from actual surface reflections (e.g., the brightly reflective soils of the semiarid regions). Individual leaves are approximated by uniformly distributed isotropic scatterers with a single scattering albedo of  $\omega$ , i.e., the intensity of the energy flux scattered by the scattering center is the same in all directions. With no dependence on direction of the radiation leaving a scattering center, the mutual shading effects alone

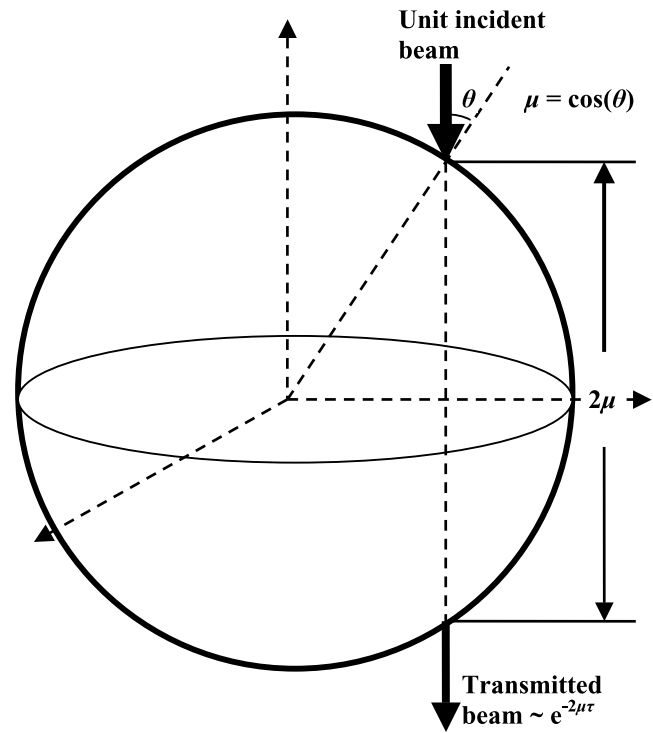


**Figure 1.** A sketch of the geometry of incident and transmitted beam of radiation for a unit sphere, where  $\tau$  is the optical depth along a radius, and  $\mu = \cos(\theta)$ , where  $\theta$  is the angle between the point of entry and the sphere axis along the direction of the incident radiation.

impose directionality on the radiation scattered outward from the sphere.

[9] Canopy optical depths in the vertical direction have been commonly assumed to be independent of the horizontal coordinates (i.e., an assumption of horizontal homogeneity is made). With this assumption, the optical path of incident radiation depends only on a vertical optical depth  $\tau_V$  and on the cosine of the angle made by the entering radiation with a normal to a horizontal plane  $\mu_{sun}$ , i.e., the optical path of radiation incoming at a slant is then  $\tau_V/\mu_{sun}$ . Scattered radiation depends also on its outward direction whose cosine relative to the vertical is  $\mu_{out}$ .

[10] For scattering from a sphere, the above incoming and outgoing directions are still relevant. However, the local optical depths of incident radiation do not depend on sun direction but rather on the location of an entering ray on the sphere relative to the axis of the sphere in the direction of the sun. Figure 1 shows how this location is characterized by the angle made by a normal to the sphere at the entering point relative to the above mentioned axis of the sphere.

[11] The incident radiation that is scattered per unit solid angle is denoted  $\Psi$  and in normalized form by the symbol  $\Phi$ , i.e.

$$\Psi(\mu_{out}, \tau, \omega) = \omega \cdot \Phi(\mu_{out}, \tau, \omega) / (4\pi). \quad (1)$$

The term  $\Phi(\mu_{out}, \tau, \omega)$  is a normalized scattering phase function and depends on  $\omega$  only at higher orders of scattering. Its single scattering value  $\Phi = \Phi_{1s}$  will depend

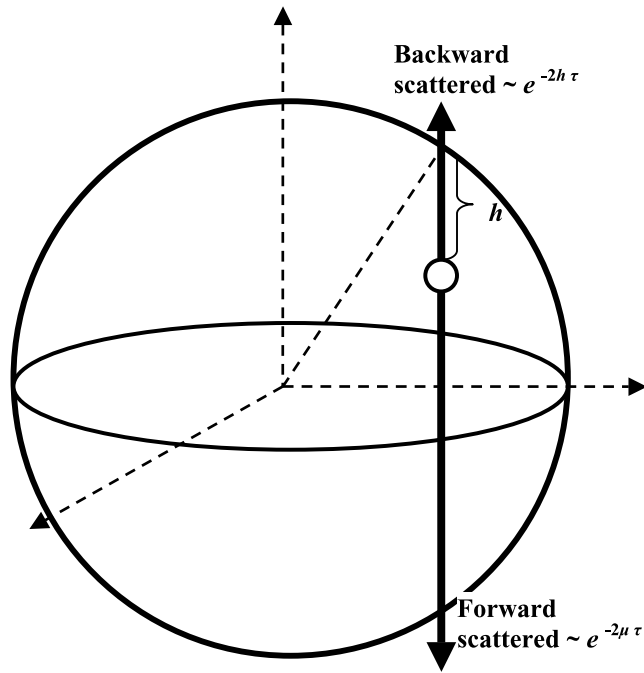


**Figure 2.** A sketch of the single scattered paths accompanying the unit incident beam of radiation shown in Figure 1. The variable  $h$  measures the distance through the sphere from entry point. The small circle is an individual volume from which the scattering originates.

only on  $\tau$ , and in the limit of small  $\tau$ , this dependence is linear, i.e.,

$$\Phi \rightarrow \Phi_{1s} \rightarrow 4\tau/3 = \tau_v. \quad (2)$$

[12] With additional scatters, less radiation is scattered per unit  $\tau$  from the sphere than that given by equation (2) because of the mutual shadowing of the scatters. Such reduction depends on the direction of the scattered radiation relative to the direction of incidence. The intensity of radiation incident on a scatterer will be reduced exponentially by the intervening scatters along the path of incidence. Scatterers near the point of entry will see the highest intensities and those deep in the sphere will see little light. Thus, the lowest exiting intensities of scattered radiation are those in the forward direction out the shaded side of the sphere, and the highest in the backward direction. With  $\tau$  larger than about 2, the backward scattered intensities approach a saturation value independent of  $\tau$ , and the forward scattered intensities decline with larger  $\tau$  to small values.

[13] The above qualitative statements apply to either a 3-D or a 1-D system. Their quantification for a 3-D geometry requires integration over all the different paths that a photon might travel. These integrations are analytic if the exponential attenuation along the photon path can be separated from spatial averaging as possible for a sphere or spheroid and for the cases of direct beam transmission and for scattering in the forward and backward directions (as shown schematically in Figure 2). A relatively exact treatment of scattering in other directions is only possible in the asymptotic limits

of small and large  $\tau$  but otherwise requires numerical quadrature. However, the numerical treatment reveals a close correspondence to that inferred from the analytic solutions as is shown in the next section. The analysis provided by these solutions shows qualitative and quantitative differences from those for a 1-D system.

### 3. Derivation of Analytic Solutions for the Single Scattering Phase Function of a Sphere

[14] Analytic integrations are done over a volume, consisting of along path (see Figure 2) and cross path integrals (the latter over a hemisphere with area increments normal to the direction of the path). In the limit of small  $\tau$ , as already discussed, the scattering is linear in  $\tau$  and the integrals reduce to a volume integration. The integration elements are clarified by developing these volume integrals. With larger  $\tau$ , it becomes necessary to include within the integration the exponential attenuation over the paths of incidence and scattering.

[15] Let  $\tau_p$  denote the optical depth for a single path in the vertical direction through the sphere, i.e., in the direction of the incident radiation. The directional angle for scattering is 0 for the backward direction, i.e.,  $\mu_{out} = 1$  in the backward direction,  $\mu_{out} = 0$  in the sideways direction, and  $\mu_{out} = -1$  in the forward direction. For a homogeneous distribution of scatters, an optical depth increment is a geometric distance increment multiplied by  $\tau$ . The geometric non-dimensional distance of the path of a vertically incident ray through a unit sphere is  $2\mu$  where  $\mu$  (see Figure 1) is the projection of the normal to the sphere onto the direction of the path. It characterizes a location on the sphere, and is not the direction of incident or scattered radiation. Thus,

$$\tau_p = \tau \int_0^{2\mu} dh = 2\mu\tau, \quad (3)$$

where the parameter  $h$  is the geometric distance along the path from the point of entry.

[16] The volume of the sphere is given by the integration of the product of the above geometric distance  $2\mu$  and area increments on the surface of the sphere projected on a surface normal to the path. The incident flux intensity per unit area consists of the total flux intercepted by the sphere divided by the total projected area of the sphere, i.e., the area of its bisecting plane. A surface integration element reduces to  $\mu d\mu$ , (i.e., an element of surface area on the sphere multiplied by its projection normal to the direction of the radiation). Averaging is applied by multiplying it by 2, i.e., the inverse of its integral. The average over the sphere of the optical depths is thus:

$$\tau_v = \int_0^1 (2\mu\tau) 2\mu d\mu = \frac{4}{3}\tau, \quad (4)$$

i.e., it is the volume optical depth that was introduced earlier in equation (2). The normalized scattering for an optically thin media is simply the volume average, equation (4). For an optically thick media it has the same integral as equations (3) and (4) but with an integrand that is the product of the transmission of the incoming and outgoing radiation

intensities, i.e., the contribution to  $\Phi_{1s}(1, \tau)$  from a path entry point on the sphere at  $\mu$  is denoted  $\varphi_b(\mu, \tau)$  and evaluated as:

$$\varphi_b(\mu, \tau) = \tau \int_0^{2\mu} \exp(-2h \cdot \tau) dh = 0.5 \cdot [1. - \exp(-4\mu\tau)], \quad (5)$$

(the  $2h$  and  $4\mu$  in the exponents are, respectively, the geometric paths to a single element in and back, and the longest path of scattering, going from one surface of the sphere to the opposite surface and back). The corresponding path integral for forward scattering  $\varphi_f(\mu, \tau)$  is simply

$$\varphi_f(\mu, \tau) = \tau_p \exp(-2\mu\tau), \quad (6)$$

where  $\tau_p$  is the path length given by equation (3). In this case, the attenuation factor (product of that for incoming and outgoing paths) is the same for scattering anywhere along the path independent of the location of the scattering element, i.e., the total path length is the same for scattering from any element at  $\mu$ . Expanded in Taylor series, both equations (5) and (6) have leading terms that are the  $\tau_p$  of equation (3).

[17] For determining the interactions with an underlying surface, the direct beam transmission  $T(\tau)$  is also needed. At one location of incident radiation it is simply the radiation intensity  $\exp(-2\mu\tau)$  (see Figure 1). Averaged with the projected area, this factor integrates to:

$$\begin{aligned} T(\tau) &= 2 \int_0^1 \mu \exp(-2\mu\tau) d\mu \\ &= 0.5\tau^{-2} [1. - (1. + 2\tau) \exp(-2\tau)]. \end{aligned} \quad (7)$$

This term also gives us the needed integration of equation (5) for the backward scattering, i.e.,

$$\Phi_{1s}(1, \tau) = \int_0^1 \varphi_b(\mu, \tau) 2\mu d\mu = 0.5 [1. - T(2\tau)]. \quad (8a)$$

[18] The integration of equation (6) to obtain the forward scattering is a bit more complicated as the weighting of the exponential attenuation term is proportional to  $\mu^2$ ,

$$\begin{aligned} \Phi_{1s}(-1, \tau) &= \int_0^1 \varphi_f(\mu, \tau) 2\mu d\mu \\ &= \tau^{-2} [1. - (1. + 2\tau + 2\tau^2) \exp(-2\tau)]. \end{aligned} \quad (8b)$$

[19] Equations (8a) and (8b) and the scattering in all other directions reduce to the same limiting expression as  $\tau \rightarrow 0$ :

$$\Phi_{1s}(\mu_{out}, \tau) \rightarrow \frac{4}{3}\tau - 2\tau^2 = \tau_v \left[ 1 - \frac{9}{8}\tau_v \right], \quad (9)$$

where the leading term (as previously indicated in equation (2)) is the volume averaged optical depth  $\tau_v$ , and the next term of the expression given in square brackets indicates that radiation is attenuated by 9/16 the volume optical depth upon entry and 9/16 upon exit. This factor exceeds 1/2

because of greater attenuation along central paths that have greater weight in the integration.

[20] The forward and backward scattering phase functions are shown in Figure 3. The behavior of these terms for large  $\tau$  is simply that obtained from equations (8a) and (8b) with the exponential terms neglected, i.e., 0.5 for the backward scattering and  $\tau^{-2}$  for the forward scattering. In this large  $\tau$  limit, the radiation will only interact within a thin shell near the edge of the sphere, and the single-scattering in any direction can be reduced to the integration over angle. This non-exponential asymptotic limit is contributed by the radiation leaking through the sides of the sphere and for any direction but downward a constant nonzero limit is approached. In particular, this integration reduces to 1/4 when  $\mu_{out} = 0$  for sideways scattering.

#### 4. Numerical Results

[21] Because analytic solutions for scattering from a sphere are only possible for  $\mu_{out} = 1$ , or  $\mu_{out} = -1$ , (or for asymptotic limits in  $\tau$ ), numerical results for these and other directions are obtained (Figure 3). The numerical solutions for the forward and backward scattering adequately reproduce the analytical solutions (see Figures 3b and 3c). The parameter space of interest is that of  $\tau \leq 3$ . Figure 4 shows the numerical solutions for normalized scattering phase function,  $\Phi_{1s}(\mu_{out}, \tau)$  versus  $\mu_{out}$ , at several values of  $\tau$ . The forward scattering peaks between 0.5 and 1.0, as seen in Figure 3, but peak values shift to between  $\tau = 1$  and 2 for sideways scattering, i.e.,  $\mu_{out} = 0$ . Only in the backward direction does the scattering continue to grow with larger  $\tau$ , resulting mathematically from the  $\tau$ -dependent term of the backward scattering being negative but that of the forward term positive. The peak scattering in other directions at intermediate optical depths results physically from the deeply penetrating photons at intermediate  $\tau$  being able to escape upward through the sides of the sphere, a unique phenomenon from the 3-D geometry. Such escaping photons would undergo much greater absorption in 1-D.

[22] These integrations establish that the scattering in all directions is approximated with errors of order of 1% or less by a linear combination of the forward and backward scattering functions, i.e., written in terms of average and differences of the backward and forward functions, i.e., equation (10c),

$$\Phi_{av}(\tau) = 0.5[\Phi_{1s}(1, \tau) + \Phi_{1s}(-1, \tau)], \quad (10a)$$

$$\Phi_{diff}(\tau) = 0.5[\Phi_{1s}(1, \tau) - \Phi_{1s}(-1, \tau)], \quad (10b)$$

$$\Phi_{1s}(\mu_{out}, \tau) = \Phi_{av} + \mu_{out} \Phi_{diff}. \quad (10c)$$

Some further improvement can be obtained by multiplying the last term in equation (10c) by a small empirical correction term  $\Phi'$ ,

$$\Phi_{1s}(\mu_{out}, \tau) = \Phi_{av} + \mu_{out} \Phi_{diff} (1 + \Phi'(\tau, \mu_{out})). \quad (11)$$

[23] The  $\Phi'$  was assumed to be of the form:  $\Phi'(\tau, \mu_{out}) = [a(1 - \mu_{out}^2)(1 - b\tau)\tau^2]/(1 - c\tau^3)$ , and optimized to

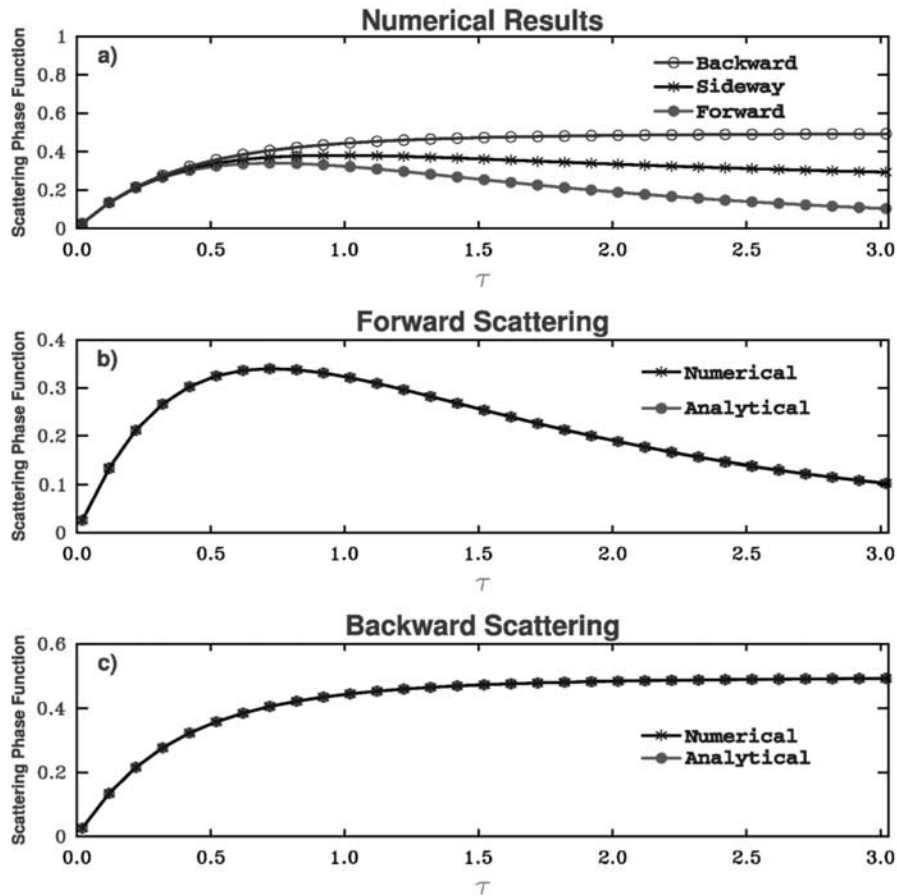


**Figure 3.** (a) The backward, forward, and sideways scattering phase function versus  $\tau$  for the spherical bush. The scattering phase function was normalized by dividing by  $0.25 \omega/\pi$ , so that the backward goes to 0.5 at large  $\tau$ . The results are obtained numerically. (b and c) Compares respectively the forward and backward scattering between the numerical and analytical solutions. They are graphically indistinguishable.

correct for the nonlinear dependence of  $\Phi$  on  $\mu_{out}$  seen for large  $\tau$ , as illustrated by Figure 5. It was constrained to match the analytic solutions at  $\mu_{out} = 1, -1$  and the large  $\tau$  results at  $\mu_{out} = 0$ . Parameter values obtained from the

fitting are  $a = -0.016989, b = -3.776098, c = -11.097930$ , respectively. The numerical solution with this correction term (i.e., equation (11)) or without (i.e., equation (10c)) are identical, as constructed, for the forward and backward

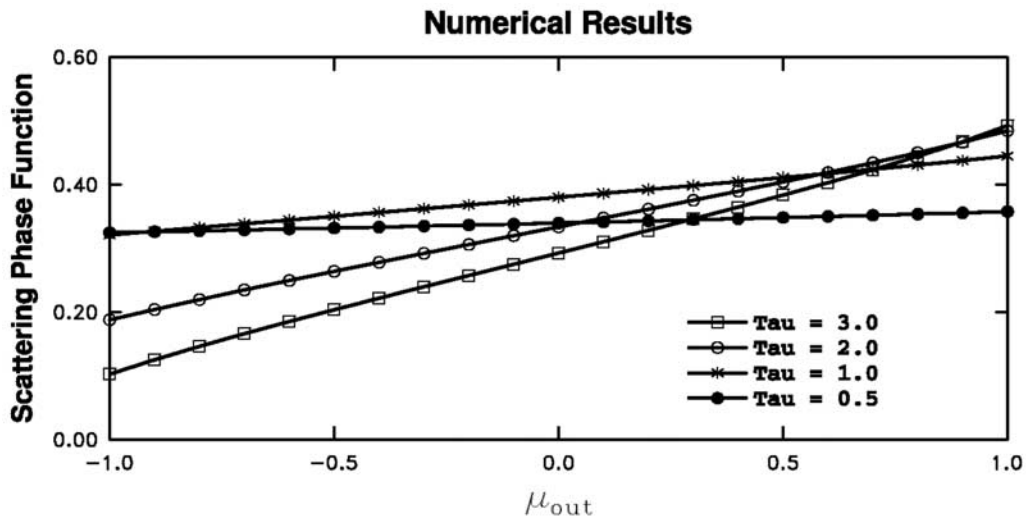


**Figure 4.** Normalized scattering function versus  $\mu_{out}$  at values of  $\tau = 0.5, 1, 2, 3$ .

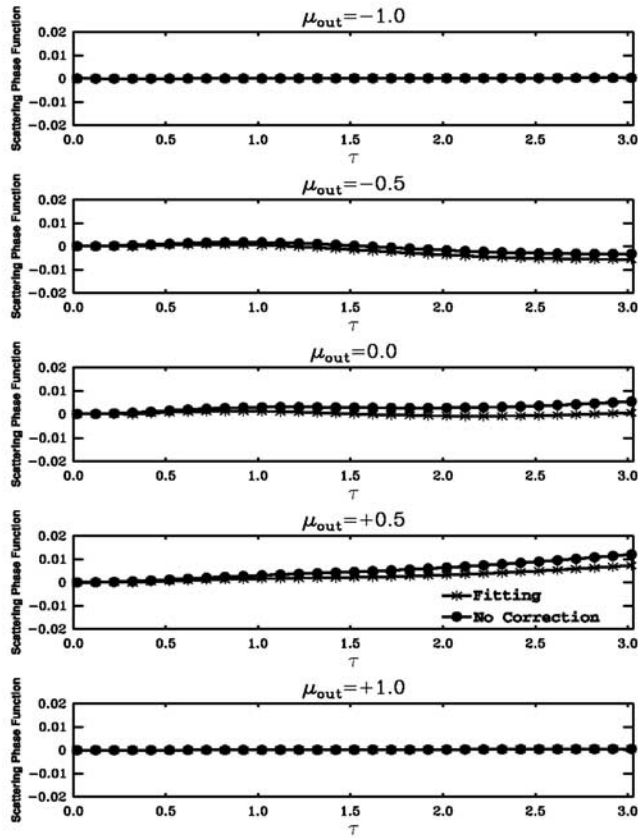


**Figure 5.** The difference between the analytical and numerical solution at values of  $\mu_{out} = -1, 0.5, 0, 0.5, 1$ , respectively, and its improvement with the fitting described in the text.

scattering (see Figures 5a and 5e) but differ with increasing  $\tau$  in other directions (Figures 5b–5d).

## 5. Application to Albedos

[24] The scattering phase function gives the fraction of incident energy escaping into a given solid angle. Albedo is the integral over this energy in the upward direction and diffuse transmission is the integral in the downward direction. Such integration is done very simply with the homogeneous scattering model, and may be extended to include leaf orientation effects.

[25] Normalized albedo  $\alpha$  or diffuse transmission  $T_d$  are  $\int \Phi d\mu_{out}$  where the integration is over the upward hemisphere for the albedo and the downward hemisphere for the diffuse transmission. These are to be multiplied by a  $0.5 \omega$  factor after accounting for a  $2\pi$  from the azimuthal integration to obtain the non-normalized conventional terms. These terms refer to averages over the area shadowed by the geometric bush. They could be divided by  $1/\mu_{sun}$  to refer to the vertical projection of the bush as conventionally done for plane parallel geometries. The appropriate integration limits are most obvious for the case of overhead sun, i.e., simply from 0 to 1 and  $-1$  to 0 respectively. The normalized single-scattering albedo  $\alpha_{1s}$  from integrating equation (11) is then:

$$\alpha_{1s} = \Phi_{av} + 0.5\Phi_{diff} = 0.75\Phi_{1s}(1, \tau) + 0.25\Phi_{1s}(-1, \tau), \quad (12)$$

and the diffuse transmission the same but with a minus sign on the  $0.5 \Phi_{diff}$  factor. For the sun at an angle, there is a sector on the bottom half of the sphere relative to the direction of the sun that scatters in the upward direction relative to the vertical, and a sector on the top half of the sphere relative to an axis toward the sun that scatters downward. With these complications:

$$\alpha = \Phi_{av} + 0.5\mu_{sun}^2 \Phi_{diff}, \quad (13)$$

$$T_d = \Phi_{av} - 0.5\mu_{sun}^2 \Phi_{diff}. \quad (14)$$

[26] Figures 6 and 7 show the dependence of this normalized albedo on the optical depth parameter  $\tau$  and on the cosine of solar zenith angle  $\mu_{sun}$ , either versus  $\tau$  at several values of  $\mu_{sun}$  (Figure 6) or versus  $\mu_{sun}$  at several values of  $\tau$  (Figure 7). From equation (15), the normalized bush albedo for overhead sun is  $0.75 \Phi_{1s}(1, \tau) + 0.25 \Phi_{1s}(-1, \tau)$ . Consistent with Figures 4 and 5, both terms are comparable at  $\tau = 0.5$  and  $\alpha \approx \Phi_{1s}(\mu, \tau) \approx 0.33$ . However, at  $\tau = 3$ ,  $\Phi_{1s}(-1, \tau) \approx 0.1$ , and  $\Phi_{1s}(1, \tau) \approx 0.5$ , so  $\alpha \approx 0.4$ . Because the albedo includes some sideways scattered photons, it only increases by 0.07 from  $\tau = 0.5$  to  $\tau = 3$  compared to the 0.17 increase of  $\Phi_{1s}(1, \tau)$ . The changes of  $\alpha$  with  $\tau$  are even smaller at lower solar zenith angle as seen in Figures 6 and 7.

[27] The normalized albedo  $\alpha$  of the sphere translates to a domain averaged albedo  $\alpha_D$  for spheres that are widely spaced relative to their size and over a black background as:

$$\alpha_D = 0.5\omega\mu_{sun}^{-1}f_c\alpha, \quad (15)$$

where  $f_c$  is the fractional coverage of the spheres. The cosine factor  $\mu_{sun}^{-1}$  can either be interpreted as multiplying  $f_c$  to get the fractional shadowed area or as the radiation crossing a horizontal surface per unit area from the unit source incident at an angle  $\theta_{sun} = \cos^{-1}\mu_{sun}$ .

## 6. Discussion

[28] This paper models the scattering properties of an isolated spherical bush. By itself, such a model would be of limited applicability. However, its simplicity facilitates its extension to more complicated situations. Its primary purpose is to serve as one of the building blocks that are needed to equip climate models with more appropriate descriptions of terrestrial radiation. However, it also provides simple insights as to the modification expected to the albedo of a collection of absorbing point scatters from 3-D geometric effects.

[29] For an overhead sun and backward reflected radiation, the integration for single scattered radiation is the same for 1-D as for 3-D, and so the 3-D reflection only differs in being a weighted average over a distribution of paths through the sphere. The fraction of radiation that is upscattered in both 1-D and 3-D systems then approaches  $0.25\omega$  for large  $\tau$  after removing the normalization. However, at other angles the fraction of photons exiting is qualitatively and quantitatively different in 3-D. In 1-D, the maximum scattering occurs in the limit of large  $\tau$  for any escape angle. Removing leaves simply reduces the accessible scattering

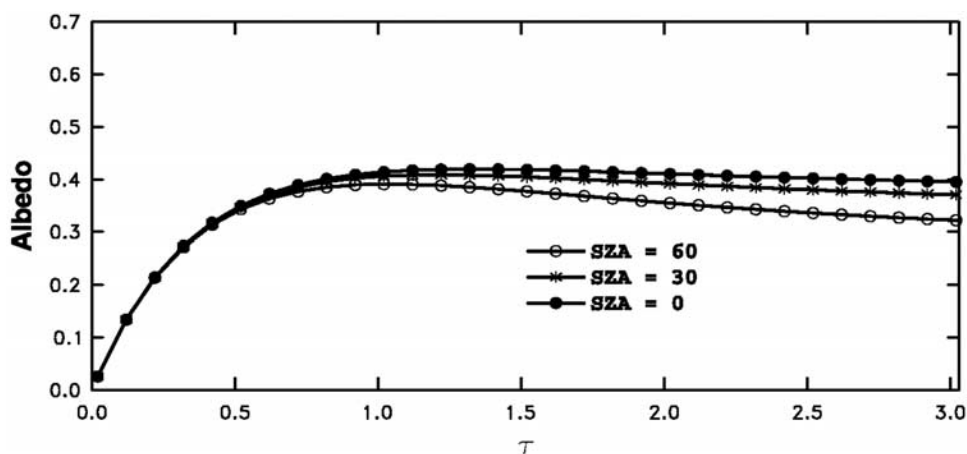


**Figure 6.** Normalized albedo. The albedo is defined as the fraction of radiation reflected by the bush from its shadowed area versus  $\tau$  for various solar zenith angles: overhead,  $30^\circ$ , and  $60^\circ$ .

surfaces and increases the leakage (transmission) out the bottom. However, in 3-D, the maximum scattering occurs at moderate optical depths, i.e.,  $\tau$  in the range of approximately 0.5 to 1.5. Under these conditions, photons can scatter throughout the sphere with their shorter escape paths more than compensating for the nonzero downward transmission. Adding more scatters above  $\tau$  of about 1.5 increases the attenuation along escape paths to reduce the overall scattering. However, even systems with very large  $\tau$  scatter more if they are spherical than if plane parallel because of sideways leakage. As shown in Figure 7, the normalized albedo reduces to 0.375 for  $\tau \rightarrow \infty$ . The comparable computation for a plane parallel system, e.g., as derived by Dickinson [1983], approaches a value of  $(1 - \log 2) \approx 0.307$ , which is smaller than the 3-D result by 24%.

[30] The integration needed for its application to albedo as described above is easily done including leaf orientation effects or for bi-Lambertian optical properties of leaves, i.e., that have transmissivities and reflectivities that differ, by representing the leaf scattering phase functions by polynomials in the cosine of the angle between incident and outward scattered radiation, e.g., equation (10) of Dickinson *et al.* [1990] and Joseph *et al.* [1996]. Spheres can be easily

extended to ellipsoids [Li and Strahler, 1992; Li *et al.*, 1995; Strahler and Jupp, 1991] and they can be described by a statistical distribution of spacing. For sparsely spaced spheres over a bright surface, the albedo obtained by combining radiation scattered by the sphere with that of the underlying surface is much more determined by geometric shading effects than by the multiple exchanges of radiation with the underlying surface implicit in the 1-D models. With these shading effects adequately characterized, the model described here should provide a much more accurate description of the partitioning of absorbed radiation between canopy and surface for the sparse shrub vegetation of semiarid systems than that now used in climate models. Differences from current 1-D treatments may be less for shorter vegetation such as grasses.

## 7. Conclusions

[31] Climate models use 1-D modeling for determining how much radiation is absorbed by canopies and their underlying surfaces. Such modeling is unrealistic in its details. This paper describes simple analytic expressions for a model of solar radiation incident on a 3-D canopy. The

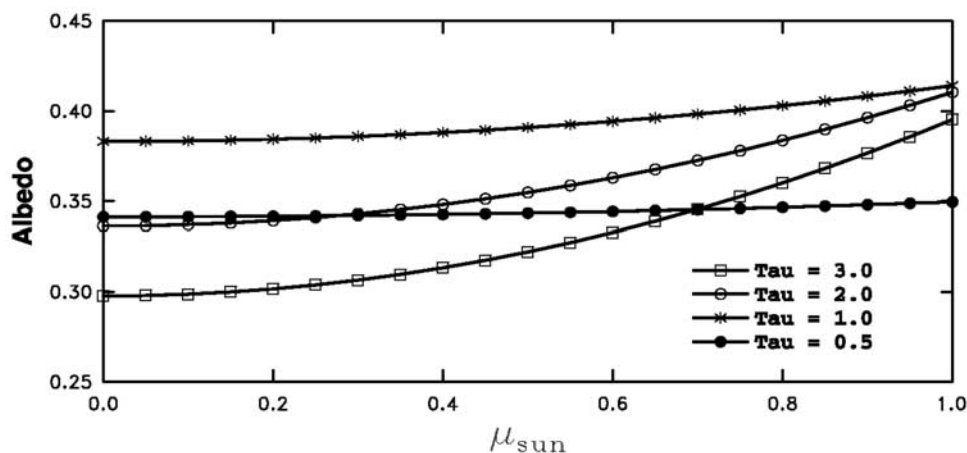


**Figure 7.** Normalized albedo versus cosine of solar zenith angles for values of  $\tau = 0.5, 1, 2$  and  $3$ .

canopy is idealized as a 3-D spherical object consisting of the simplest individual scattering centers. This spherical bush is viewed as a building block for the construction of more complex models of the interaction of incident radiation with more realistic canopy configurations. It is treated without the complications of multiple scattering, leaf orientation effects, or of an underlying surface. With such simplification, the paper is able to provide a complete analytic description of the directional scattering and its integration to an albedo. The solutions are obtained by integrations over a distribution of optical paths through the sphere. Exact solutions are obtained for the transmission of the direct beam, and for the backward and forward single-scattered components. These terms alone are shown to be sufficient to provide a complete scattering phase function, and sun-angle dependent albedos. Scattering is substantially enhanced for radiation leaving in near horizontal directions compared to that from 1-D modeling, and thus also albedos, especially for leaf area index in the range of 1 to 3. Multiple-scattering can be included using these building blocks with some further approximation [Dickinson, 2008]. For use in a climate model, these solutions must be combined with radiative interactions between different bush elements and with an underlying surface, and with a characterization of the angle dependences imposed by leaf-orientations.

[32] **Acknowledgments.** This study was supported in part by the lead author's NSF grant ATM-0720619 and DOE grant DE-FG02-01ER63198.

## References

- Betts, R. A., P. D. Falloon, K. K. Goldewijk, and N. Ramankutty (2007), Biogeophysical effects of land use on climate: Model simulations of radiative forcing and large-scale temperature change, *Agric. For. Meteorol.*, *42*(2–4), 216–233, doi:10.1016/j.agrformet.2006.08.021.
- Bonan, G. B., D. Pollard, and S. L. Thompson (1992), Effects of boreal forest vegetation on global climate, *Nature*, *359*(6397), 716–718, doi:10.1038/359716a0.
- Dickinson, R. E. (1983), Land surface processes and climate-surface albedos and energy balance, *Adv. Geophys.*, *25*, 305–353.
- Dickinson, R. E. (2008), Determination for climate models of the multi-scattered solar radiation from a canopy with leaves modeled as a 3D distribution of homogeneous isotropic scatters, *J. Comput. Phys.*, *227*, 3667–3677, doi:10.1016/j.jcp.2007.12.010.
- Dickinson, R. E., B. Pinty, and M. M. Verstraete (1990), Relating surface albedos in GCM remotely sensed data, *Agric. For. Meteorol.*, *52*, 109–131, doi:10.1016/0168-1923(90)90103-D.
- Govaerts, Y., and M. M. Verstraete (1998), Raytran: A Monte Carlo ray tracing model to compute light scattering in three-dimensional heterogeneous media, *IEEE Trans. Geosci. Remote Sens.*, *36*, 493–505, doi:10.1109/36.662732.
- Huang, D., et al. (2007a), Canopy spectral invariants for remote sensing and model applications, *Remote Sens. Environ.*, *106*, 106–122, doi:10.1016/j.rse.2006.08.001.
- Huang, D., Y. Knyazikhin, W. Wang, D. W. Deering, P. Stenberg, N. Shabanov, B. Tan, and R. Myneni (2007b), Stochastic transport theory for investigating the three-dimensional canopy structure from space measurements, *Remote Sens. Environ.*, doi:10.1016/j.rse.2006.05.026.
- Joseph, J. H., J. Iaquina, and B. Pinty (1996), The use of two-stream approximations for the parameterization of solar radiative energy fluxes through vegetation, *J. Clim.*, *9*, 2326–2336, doi:10.1175/1520-0442(1996)009<2326:TUOTSA>2.0.CO;2.
- Kimes, D., J. Gastellu-Etchegorry, and P. Esteve (2002), Recovery of forest canopy characteristics through inversion of a complex 3D model, *Remote Sens. Environ.*, *79*(2), 320–328, doi:10.1016/S0034-4257(01)00282-6.
- Knyazikhin, Y., J. V. Martonchik, R. B. Myneni, D. J. Diner, and S. W. Running (1998), Synergistic algorithm for estimating vegetation canopy leaf area index and fraction of absorbed photosynthetically active radiation from MODIS and MISR data, *J. Geophys. Res.*, *103*(D24), 32,257–32,276, doi:10.1029/98JD02462.
- Knyazikhin, Y., A. Marshak, and R. B. Myneni (2005), Three-dimensional radiative transfer in vegetation canopies and cloud-vegetation interaction, in *Three-Dimensional Radiative Transfer in the Cloudy Atmosphere*, edited by A. Marshak and A. B. Davis, pp. 617–652, Springer, New York.
- Lawrence, P. J., and T. N. Chase (2007), Representing a new MODIS consistent land surface in the Community Land Model (CLM 3.0), *J. Geophys. Res.*, *112*, G01023, doi:10.1029/2006JG000168.
- Lewis, P. (1999), Three-dimensional plant modelling for remote sensing simulation studies using the Botanical Plant Modelling System, *Agronomy*, *19*(3/4), 185–210, doi:10.1051/agro:19990302.
- Li, X., and A. H. Strahler (1992), Geometric-optical bidirectional reflectance modeling of the discrete crown vegetation canopy: Effect of crown shape and mutual shadowing, *IEEE Trans. Geosci. Remote Sens.*, *30*, 276–292, doi:10.1109/36.134078.
- Li, X., A. H. Strahler, and C. E. Woodcock (1995), A hybrid geometric optical-radiative transfer approach for modeling albedo and directional reflectance of discontinuous canopies, *IEEE Trans. Geosci. Remote Sens.*, *33*(2), 466–480, doi:10.1109/36.377947.
- Liang, X.-Z., et al. (2005), Development of Land Surface Albedo Parameterization Based on Moderate Resolution Imaging Spectroradiometer (MODIS) data, *J. Geophys. Res.*, *110*, D11107, doi:10.1029/2004JD005579.
- Lucht, W., C. B. Schaaf, and A. H. Strahler (2000), An algorithm for the retrieval of albedo from space using semiempirical BRDF models, *IEEE Trans. Geosci. Remote Sens.*, *38*(2), 977–998, doi:10.1109/36.841980.
- Myneni, R. B., S. Maggion, J. Iaquina, J. L. Privette, N. Gobron, B. Pinty, M. M. Verstraete, D. S. Kimes, and D. L. Williams (1995), Optical remote sensing of vegetation: Modeling, caveats, and algorithms, *Remote Sens. Environ.*, *51*(1), 169–188, doi:10.1016/0034-4257(94)00073-V.
- Petty, G. W. (2002), Area-average solar radiative transfer in three-dimensionally inhomogeneous clouds: The Independently Scattering Cloudlet model, *J. Atmos. Sci.*, *59*, 2910–2929, doi:10.1175/1520-0469(2002)059<2910:AASRTI>2.0.CO;2.
- Pinty, B., T. Lavergne, R. E. Dickinson, J.-L. Widlowski, N. Gobron, and M. M. Verstraete (2006), Simplifying the interaction of land surfaces with radiation for relating remote sensing products to climate models, *J. Geophys. Res.*, *111*, D02116, doi:10.1029/2005JD005952.
- Qin, W., and S. A. W. Gerstl (2000), 3-D scene modeling of semidesert vegetation cover and its radiation regime, *Remote Sens. Environ.*, *74*(1), 145–162, doi:10.1016/S0034-4257(00)00129-2.
- Schaaf, C. B., et al. (2002), First operational BRDF, albedo and nadir reflectance products from MODIS, *Remote Sens. Environ.*, *83*, 135–148, doi:10.1016/S0034-4257(02)00091-3.
- Sellers, P. J. (1985), Canopy reflectance, photosynthesis and transpiration, *Int. J. Remote Sens.*, *6*, 1335–1372, doi:10.1080/01431168508948283.
- Shabanov, N. V., Y. Knyazikhin, F. Baret, and R. B. Myneni (2000), Stochastic modeling of radiation regime in discontinuous vegetation canopies, *Remote Sens. Environ.*, *74*, 125–144, doi:10.1016/S0034-4257(00)00128-0.
- Strahler, A. H., and D. L. B. Jupp (1991), Geometric-optical modeling of forest as scenes composed of three-dimensional discrete objects, in *Photon-Vegetation Interactions: Applications in Optical Remote Sensing and Plant Ecology*, edited by R. B. Myneni and J. Ross, pp. 415–440, Springer, Heidelberg, Germany.
- Tian, Y., R. E. Dickinson, L. Zhou, R. B. Myneni, M. Friedl, C. B. Schaaf, M. Carroll, and F. Gao (2004), Land boundary conditions from MODIS data and consequences for the albedo of a climate model, *Geophys. Res. Lett.*, *31*, L05504, doi:10.1029/2003GL019104.
- Wang, Z., X. Zeng, M. Barlage, R. E. Dickinson, F. Gao, and C. B. Schaaf (2004), Using MODIS BRDF and albedo data to evaluate global model land surface albedo, *J. Hydrometeorol.*, *5*, 3–14, doi:10.1175/1525-7541(2004)005<0003:UMBAAD>2.0.CO;2.
- R. E. Dickinson, Q. Liu, and L. Zhou, School of Earth and Atmospheric Sciences, Georgia Institute of Technology, 311 Ferst Drive, Atlanta, GA 30332-0340, USA. (robted@eas.gatech.edu)
- Y. Knyazikhin and C. B. Schaaf, Department of Geography, Boston University, Boston, MA 02215, USA.
- T. Lavergne and B. Pinty, Global Environmental Monitoring Unit, Institute for Environment and Sustainability, European Commission Joint Research Centre, I-21020 Ispra, Italy.
- Y. Tian, Center for Satellite Applications and Research, NESDIS, NOAA, Camp Springs, MD 20746, USA.